# Doping dependent optical properties of $Bi_2Sr_2CaCu_2O_{8+\delta}$

**J Hwang[1], T Timusk[1,2] and G D Gu[3]**

[1]Department of Physics and Astronomy, McMaster University, Hamilton, ON L8S 4M1, Canada
[2]The Canadian Institute of Advanced Research, Toronto, Ontario M5G 1Z8, Canada
[3]Department of Physics, Brookhaven National Laboratory, Upton, NY 11973-5000, USA

E-mail: hwangjs@mcmaster.ca

**Abstract.** We report on the ab-plane reflectance of the high temperature superconductor $Bi_2Sr_2CaCu_2O_{8+\delta}$ (Bi-2212). Samples spanning the doping range from under doped with $T_c$ = 67 K(UD), to optimally doped with $T_c$ =96 K (OPT), to over doped with $T_c$ =60 K (OD) were measured from room temperature down to the superconducting state. The measured reflectance data were analyzed to extract the optical conductivity and the real and imaginary parts of the free carrier optical self-energy. We get an estimate of the dc resistivity from the low frequency extrapolation of the optical conductivity and the superfluid density from the imaginary part of the optical conductivity. The conductivity sum rule can be related to the changes of the kinetic energy of the system. When this system becomes a superconductor, the kinetic energy decreases in the underdoped samples and increases in overdoped ones. The optical self-energy, obtained from the extended Drude model, is dominated by two channels of interaction, a sharp mode and a broad background. The amplitude of the mode is strongly doping and temperature dependent whereas the background decreases weakly with doping and is nearly temperature independent.

PACS numbers: 74.25.Gz, 74.62.Dh, 74.72.Hs

## 1. Introduction

Since the discovery of high-temperature superconductivity in the copper oxides [1] the dynamical properties of the charge carriers in these materials have been investigated with a variety of spectroscopic techniques. Within a certain class of theories these properties provide a direct fingerprint to the the mechanism of superconductivity. For example, if in analogy with the BCS superconductors, superconductivity is driven by the exchange of bosons, then a study of the self-energy spectrum of the superconducting current carriers would help us in identifying the relevant bosons. Traditionally this has been done with tunneling spectroscopy where numerical inversion techniques using Migdal-Eliashberg theory[2] revealed spectroscopic fingerprints in the self-energy that could be compared with the phonon densities of states determined by inelastic neutron scattering and thereby unambiguously identified as phonons [3]. The self-energy spectra of the high temperature superconductors have also been investigated with increasing success with advanced spectroscopic techniques [4] including angle resolved photoemission (ARPES), tunneling, optics and magnetic neutron scattering, but so far at least no consensus has been achieved in the interpretation of these spectra.

Contrasting with the traditional BCS mechanism of boson exchange there are alternative, exotic models of the mechanism of high temperature superconductivity involving the formation of new states at high temperature which would then Bose condense to form a superconductor as the temperature is lowered. There have also been suggestions that combine the two pictures where at low doping levels, close to the antiferromagnetic part of the phase diagram, an exotic mechanism operates but with increasing hole concentration a more conventional boson exchange takes over. To throw some light on these issues we have undertaken a study of the spectrum of excitations responsible for the self-energy of the carriers as a function of doping in the Bi-2212 system using the optical conductivity as our experimental probe. The Bi-2212 system is has several advantages for such an investigation. First the system can be doped from the moderately underdoped region with $T_c$=60 K through the optimally doped well into the overdoped region with $T_c$=60 K. Furthermore, because the crystals of this material can be vacuum cleaved, they have also been studied extensively with ARPES [5] and tunneling [6].

The extended Drude model that we use to find the real and imaginary parts of the scattering rate and the self-energy assumes that there is only one channel of conductivity and that any deviation from the Drude form is due to inelastic interactions. The validity of this assumption can be tested to some extent by comparing the scattering rate obtained from optics with the results from ARPES. When such comparisons are made the resulting self-energy spectra generally agree to an accuracy of about 15 % [7, 8]. One cannot expect any better agreement from the two methods since they measure different things, ARPES gives us the quasiparticle lifetimes and self energies for any given $k$ vector whereas the optical self-energy represents an average over the Fermi surface of contributions to the current excited by the external field with each

point characterized by a velocity component parallel to the field and a life time of this particular quasiparticle. It therefore comes as a surprise that the two methods give very similar results not only for the absolute values of these quantities but also their frequency and temperature dependencies, in particular if the ARPES results for quasiparticles near the nodal point are compared with the optical conductivity. Away from the nodes there are large discrepancies: at low temperatures ARPES quasiparticles do not show the narrowing that the optical conductivity shows and there appears to be an inelastic scattering background that is not seen in the optical conductivity.

Many optical studies have been done on the cuprate systems, especially $La_{2-x}Sr_xCuO_4$ (LSCO) and $YBa_2Cu_3O_{6+x}$ (Y123) for light polarized along the ab-plane as well as the less conducting c-axis direction.[9] Much early optical work has was also done on the important Bi-2212 material [10, 11, 12, 13]. Quijada *et al.* [12] give a complete set of references to the earliest work. However recent advances in crystal growth with image furnaces have yielded better quality crystals, suggesting a need for new studies of this material. Here we report on the optical properties of the ab-plane of Bi-2212 over a broad doping range from underdoped to overdoped at various temperatures above and below $T_c$. We obtain various optical quantities from the measured reflectance and discuss some important doping dependent issues. In particular, we focus on the doping dependent superfluid density and the doping dependence of the contributions of various excitations to the optical self-energy.

The superfluid density is a fundamentally important quantity in superconductivity because it is directly related to the ability of the superconducting wave function to resist perturbations to its phase. The superfluid density can be obtained from the optical spectrum in two ways, by analyzing the imaginary part of the conductivity as a function of frequency, or by comparing the spectral weight loss in the low frequency region as the superconducting condensate is formed, according to the Ferrell-Glover-Tinkham (FGT) sum rule [14]. Any discrepancy in the superfluid density obtained by the two methods can be related to the kinetic energy difference between normal and superconducting states. This difference can in turn be related to proposed models of the superconducting mechanism driven by kinetic energy [15, 16, 17]. Recent interest has focussed on the *doping dependence* of the superfluid density and the kinetic energy difference [16, 17].

The suggestion that spin fluctuations might provide the pairing bosons was made early by the theoretical community [18, 19]. Adding to the interest in magnetic excitations was the absence of an isotope effect in optimally doped samples and the discovery of the sharp magnetic resonance mode at 41 meV in Y123 in the magnetic susceptibility spectrum by inelastic neutron scattering [20, 21, 22, 23, 24, 25, 26, 27]. A sharp excitation at this energy can also be seen by other experimental techniques such as optical spectroscopy [8, 28, 29, 30, 31, 32], ARPES [33, 34, 35, 36, 37, 38], or tunneling [39, 40]. This excitation has the interesting property that its energy $\hbar\Omega$ is proportional to the superconducting transition temperature according to $\hbar\Omega \approx 5k_BT$ at all doping levels [26] and in all the cuprate families where large single crystals are

available. The only exception are the reduced $T_c$ systems such as LSCO where, while there is peak in the magnetic suscpeptibilty, a sharp resonance does not develop at low temperature. In the overdoped samples the magnetic resonance appears only below $T_c$ but in underdoped samples it can be seen well above $T_c$ [24, 41]. However even in these systems the resonance grows rapidly in strength at the superconducting transition. This temperature dependence of the mode can also be seen in ARPES spectra in the nodal direction [37, 42] In the view of all these connections to superconductivity it is not surprising that the role of magnetic resonance mode in superconductivity has been discussed widely [24, 43, 44, 45].

One possible connection of the magnetic resonance to superconductivity would be through its contribution to the optical and quasiparticle self-energy, where it would have a role similar to the role of phonons in BCS superconductivity [8, 30, 31, 34, 37, 46, 47, 48]. The problems with this scenario have been pointed out by several authors. In the overdoped Y123 the resonance is not present in the normal state and cannot initiate the transition at $T_c$. In the highly overdoped state the signature of the resonance vanishes from the optical conductivity at a doping level where $T_c$ is around 60 K [8, 29, 49] in both Bi-2212 and $Tl_2Ba_2CuO_{6+\delta}$ (Tl-2201). A general weakening of the contribution of the magnetic resonance to the carrier self-energy with doping has also been seen in ARPES and tunneling [37, 40, 42]. It was suggested by Hwang *et al* [8] that the coupling of the resonance disappears above a critical doping level of $p = 0.24$. Other experiments support the idea that there is a significant change in the properties of the cuprates at this doping level. Shibauchi *et al.* [50] observed that the pseudogap temperature $T^*$ in c-axis transport merged to $T_c$ in Bi-2212 system near the critical doping, 0.24. Ozyuzer *et al.* [51] have observed that there was no indication of a pseudogap near at Fermi level in their tunnelling conductance spectrum of a very overdoped Bi-2212 with $T_c$=56 K. Some ARPES studies showed that near the critical doping the topology of the Fermi surface transformed from hole-like to electron-like in Pb-doped Bi-2201 [52, 53], LSCO [54] and Bi-2212 [55]. Another ARPES study showed that a crossover two- to three-dimensional electronic structure occurred near the critical doping with $T_c$= 22 K in $(Bi,Pb)_2(Sr,La)_2CuO_{6+\delta}$ system [56], which has $T_c^{max}$= 35 K.

In addition to the sharp mode there is a continuous bosonic background spectrum that is responsible for the strong linearly rising scattering rate that extends to very high frequencies. It has been discussed in the theoretical literature in the context of models such as the marginal Fermi liquid (MFL) [57] or the interaction of the charge carriers with a continuous spectrum of spin fluctuations the Millis-Monien-Pines (MMP) spectrum [19]. This broad background exists at all temperatures and doping levels and in all cuprate systems including LSCO system [58], where there is no clear evidence for the presence of the magnetic resonance mode. This ubiquitous feature in the cuprates may be also be responsible for the broad kink feature in ARPES spectra near nodal region [59]. Other strongly correlated electron systems have similar broad backgrounds in their bosonic spectra or the real part of the optical self-energy, for an example, the sodium cobaltate system [60]. Interestingly, the sharp mode and the broad

background was captured by optical spectroscopy in early days of the high temperature of superconductors [61].

In the next section we describe our experimental technique including sample preparation. In the following section, we provide measured reflectance spectra and describe how we extract the optical conductivity from the measured reflectance. In the following section, we extract the superfluid density using two different methods and the kinetic energy change going from the normal to the superconducting state. Next, we introduce the optical self-energy using the extended Drude formalism and describe the doping and temperature dependent properties of the self-energy. In the final section, we we relate our experiments to several important recent issues and provide overall summary of our work.

## 2. Sample preparations and experiments

The Bi-2212 single crystals used in the study were grown in an optical image furnace with the traveling solvent floating-zone technique. To get the appropriately doped samples from as-grown crystals we annealed under various oxygen-annealing conditions [62]; which yielded good samples of the underdoped (UD), optimally doped (OPT), and overdoped (OD) phases. Unwanted c-axis longitudinal phonons can be admixed in ab-plane optical data of other cuprates such as LSCO and Y123 [63, 64]. We see no evidence of these in our samples. We could obtain shiny optical quality ab-plane surfaces Bi-2212 by cleaving the sample.

A commercial Fourier transform spectrometer, Bruker IFS 66v/S, was used to obtain the reflectance data over a wide frequency range from 50 to 40,000 $cm^{-1}$. For the low temperature measurements we used a continuous flow liquid Helium cryostat with an automated temperature control and sample change system [65] to improve the reproducibility over a manual system. A polished stainless steel mirror was used as an intermediate reference to correct for the instrument drift with time and temperature. An in-situ evaporated gold (50 - 14,000 $cm^{-1}$) or aluminum (12,000 - 40,000 $cm^{-1}$) film on the sample was used as the final reflectance reference [66]. The reflectance of the gold films was in turn calibrated with a polished stainless steel sample where we relied on the Drude theory and the dc resistivity as the ultimate reference. An advantage of this method is that it corrects for geometrical effects of an irregular surface. The in-situ gold evaporation technique gives accurate temperature dependent data with an accuracy better than $\pm$ 0.05 % at room temperature.

We measured reflectance of four overdoped ($T_c$ = 80 K, 82 K, 65 K, and 60 K), one optimally doped ($T_c$ = 96 K), and one underdoped ($T_c$ = 69 K) Bi-2212 sample. We estimated the hole doping levels of the samples using the empirical parabolic equation of Presland *et al.* [67]: $p(T_c) = 0.16 \mp [1/82.6\,(1 - T_c/T_c^{max})]^{1/2}$, where $T_c^{max}$ is the maximum $T_c$ of the material. The determination of $T_c^{max}$ is not an easy problem [62] as it depends on the growth conditions and dopant levels. In the absence of a better method, we use the generally accepted value of 91 K as the $T_c^{max}$ for Bi-2212. We should

mention here that our optimally-doped sample is doped with a small amount of Y to yield a relatively well ordered system and shows a surprisingly high $T_c = 96$ K [62] and we assigned $p = 0.16$ as its hole doping level. The disadvantage of the parabolic approximation is that it does not uniquely determine the doping level of the sample since there are two independent $p$ values for each value of $T_c$. To avoid the ambiguity in the determination of the doping levels we used the slope of the infrared reflectance as an additional test of the doping level [68]. Table 1 shows the estimated doping levels of our eight Bi-2212 samples.

## 3. Reflectance and optical conductivity

In this section we provide the measured reflectance and the optical conductivity derived from the reflectance by using Kramers-Kronig (KK) transformations [12, 69, 70, 71]. To use this method we have to extrapolate the measured reflectance to zero frequency on the low frequency side of the measured range and to infinite frequency on the high frequency side. We used the following extrapolations. For $\omega \to 0$, the reflectance was extrapolated by assuming a Hagen-Rubens frequency dependence, $1 - R(\omega) \propto \omega^{1/2}$ for normal states and $1 - R(\omega) \propto \omega^4$ for the superconducting states. For $\omega \to \infty$, the reflectance has been extended by using a literature data [72] and free-electron behavior ($R \propto \omega^{-4}$).

To obtain further optical constants from the measured reflectance ($R(\omega)$) and the corresponding calculated phase ($\phi(\omega)$) from KK analysis, we used the Fresnel's equation for normal incidence:

$$\frac{1 - n(\omega) - ik(\omega)}{1 + n(\omega) + ik(\omega)} = \sqrt{R(\omega)}e^{i\phi(\omega)} \tag{1}$$

or

$$n(\omega) = \frac{1 - R(\omega)}{1 + R(\omega) - 2\sqrt{R(\omega)}\cos\phi(\omega)} \tag{2}$$

$$k(\omega) = \frac{-2\sqrt{R(\omega)}\sin\phi(\omega)}{1 + R(\omega) - 2\sqrt{R(\omega)}\cos\phi(\omega)} \tag{3}$$

where $n(\omega)$ and $k(\omega)$ are the index of refraction and the extinction coefficient, respectively.

In principle, we are able to obtain any other optical quantities by using the various relationships between the optical quantities [69].

$$\epsilon_1(\omega) = n^2(\omega) - k^2(\omega) \tag{4}$$

$$\epsilon_2(\omega) = 2n(\omega)k(\omega) \tag{5}$$

and

$$\sigma(\omega) = -i\frac{\omega}{4\pi}[(\epsilon_1(\omega) - \epsilon_H) + i\epsilon_2(\omega)] \tag{6}$$

where $\epsilon_1(\omega)$ and $\epsilon_2(\omega)$ are the real and imaginary parts of the optical dielectric constant, respectively, and $\sigma(\omega) \equiv \sigma_1(\omega) + i\sigma_2(\omega)$ is the complex optical conductivity.

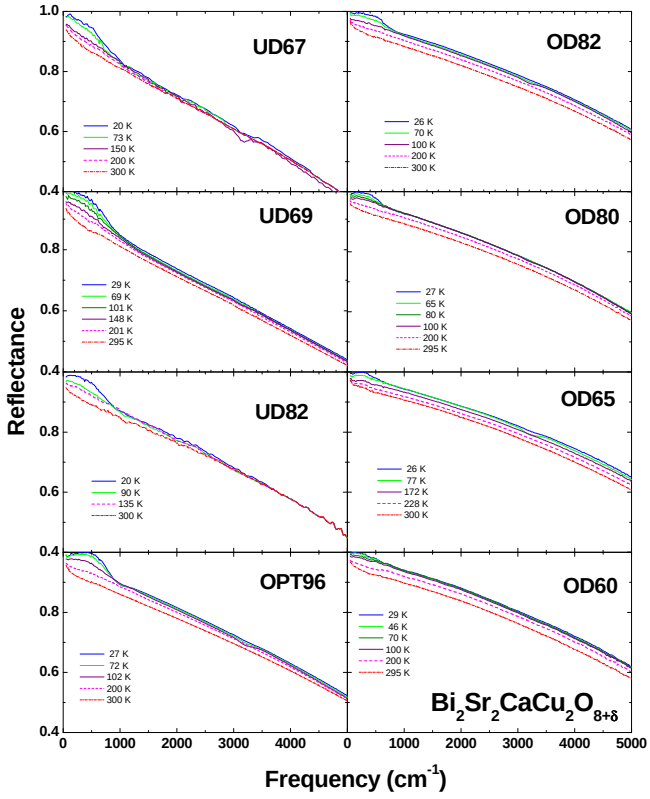


**Figure 1.** ab-plane reflectance of Bi-2212 at eight different doping levels. The overall reflectance increases as the hole doping level increases with charge carrier density introduced by doping. Here and in the following figures we use a brief notation to describe doping status of our samples, for example UD67 stands for the underdoped sample with $T_c$=67 K, OD for overdoped and OP for optimal doping. We note that a dip feature near 3300 cm$^{-1}$ of the low temperature data of some of the samples an absorption is a band from ice on the sample. This feature does not affect low frequency data below the absorption frequency, 3300 cm$^{-1}$. However it affects the high frequency data above 3300 cm$^{-1}$.

The quantity $\epsilon_H$ is the contribution to the dielectric constant from all the high frequency spectral weight but excluding the low frequency free carrier part or intraband spectral weight. It is often difficult to determine where the dividing line between the free carriers and the interband absorption lies. We take $\epsilon_H$ at a high frequency ($\sim 2eV$) for each doping level (note that there is doping dependence in $\epsilon_H$). To get $\sigma_2$ we used $\epsilon_H$ values shown in table 1. Recently, the accuracy of the various methods of finding $\epsilon_H$ has becomes an important issue because the optical scattering rate is very sensitive to the value of $\epsilon_H$, especially at high frequency (for more discussions see the following section and figure 6 and the related text).

Figure 1 displays the measured ab-plane reflectance of Bi-2212 at eight different doping levels and at various temperatures. As the hole doping level increases, some interesting doping dependent features show up; the overall reflectance level increases and the overall shape becomes more curved. For each doping level, as the temperature

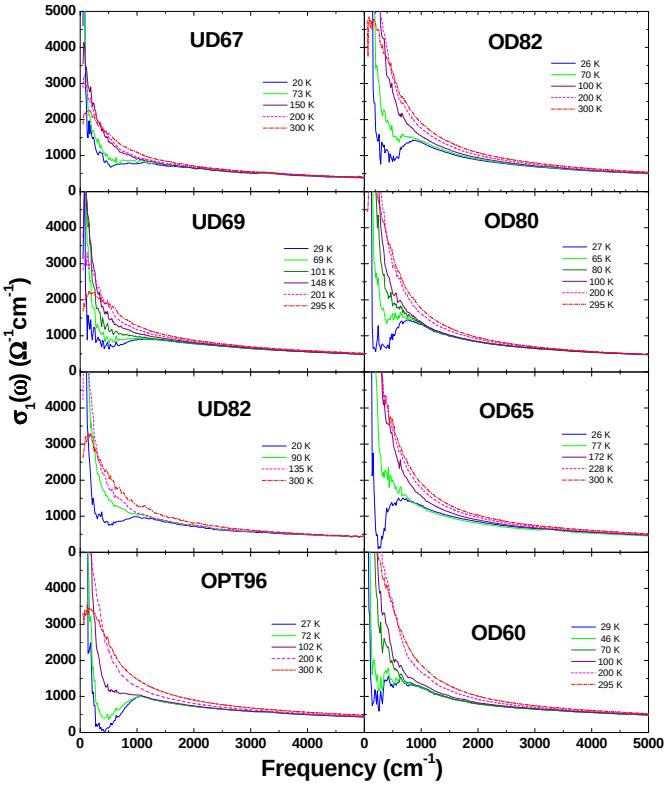


**Figure 2.** The ab-plane optical conductivity of Bi-2212 of eight Bi-2212 samples at various temperatures above and below $T_c$.

decreases the overall reflectance increases because of the reduced scattering and, more interestingly, a shoulder appears between 500 cm$^{-1}$ and 1000 cm$^{-1}$ below an onset temperature, which is also doping dependent. We will analyze the shoulder feature in detail and discuss its doping dependent properties in the section "Extended Drude model and optical self-energy". At room temperature the reflectance below 2000 cm$^{-1}$ is approximately linear in frequency. This linear variation, the so called marginal Fermi liquid behavior [57] in Bi-2212 at 300 K has been analysed in detail by Hwang *et al.* [68] below 2000 cm$^{-1}$ over a wide doping range.

Figure 2 displays the real part of the optical conductivity of Bi-2212. We observe strong temperature dependence only in low frequency region, below 3000 cm$^{-1}$. The spectral weight or the number of effective charge carriers per Cu atom on $CuO_2$ plane is defined as follows:

$$N_{eff}(\omega) = \frac{2mV_{Cu}}{\pi e^2} \int_{0^+}^{\omega} \sigma_1(\omega')d\omega' \tag{7}$$

where $m$ is the free electron mass, $V_{Cu}$ is the volume per Cu atom in the sample, $e$ is the charge of an electron, and $\sigma_1$ is the real part of the optical conductivity. The spectral weight is proportional to the area under $\sigma_1(\omega)$ curve. As the hole doping increases the overall conductivity increases. For each doping level, as the temperature decreases, the spectral weight at low frequencies increases as a result of the narrowing the Drude-like

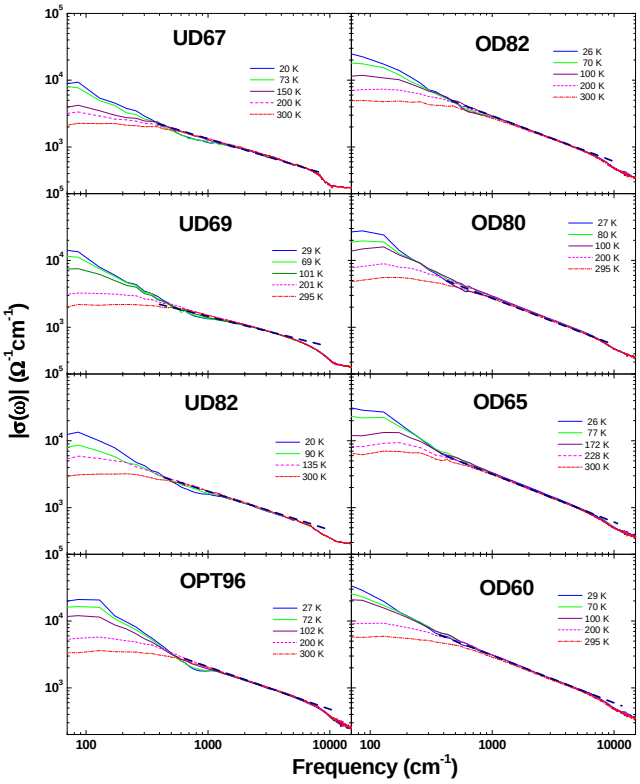


**Figure 3.** Amplitude of the optical conductivity, $|\sigma(\omega)| \equiv \sqrt{\sigma_1^2(\omega) + \sigma_2^2(\omega)}$. The dashed lines are least square fits of the temperature independent region.

absorption band near zero frequency. This shift of spectral weight continues down to the superconducting transition temperature, $T_c$. Below or near $T_c$ a strong depression of spectral weight below 1000 cm$^{-1}$ sets in and grows with decreasing temperature. This feature is related to the step-like feature in the optical scattering rate. (for more detailed discussion see Sec. "Extended Drude model and optical self-energy") The missing area between the normal and the superconducting curves can be a measure of the superfluid density (more detailed discussion see the section "FGT Sum rule, superfluid density, and kinetic energy"). Even in the superconducting state we have a sizable amount of residual spectral weight near zero frequency, which is absent in the conventional superconductors [73, 74, 75, 76].

The complex optical conductivity can be described by an amplitude and a phase, i.e. $\sigma(\omega) = |\sigma(\omega)|e^{i\Phi(\omega)}$, where $|\sigma(\omega)| = \sqrt{\sigma_1^2(\omega) + \sigma_2^2(\omega)}$, and $\Phi(\omega) = \tan^{-1}(\sigma_2(\omega)/\sigma_1(\omega))$. Anderson [77] suggested simple power law behavior for the complex optical conductivity in his Luttinger Liquid model. Recently van der Marel *et al.* [78] revisited the Anderson's model describing the optical conductivity as $\sigma(\omega) = C(-i\omega)^{\gamma-2}$, where $C$ is a frequency independent constant. In this description we have $|\sigma(\omega)| = C\omega^{\gamma-2}$ and $\Phi(\omega) = \pi/2(2-\gamma)$, which is frequency independent. Note that this formalism can describe only the temperature independent parts of the conductivity spectra. In figure 3 we plot the amplitude of the optical conductivity of our eight Bi-2212 samples

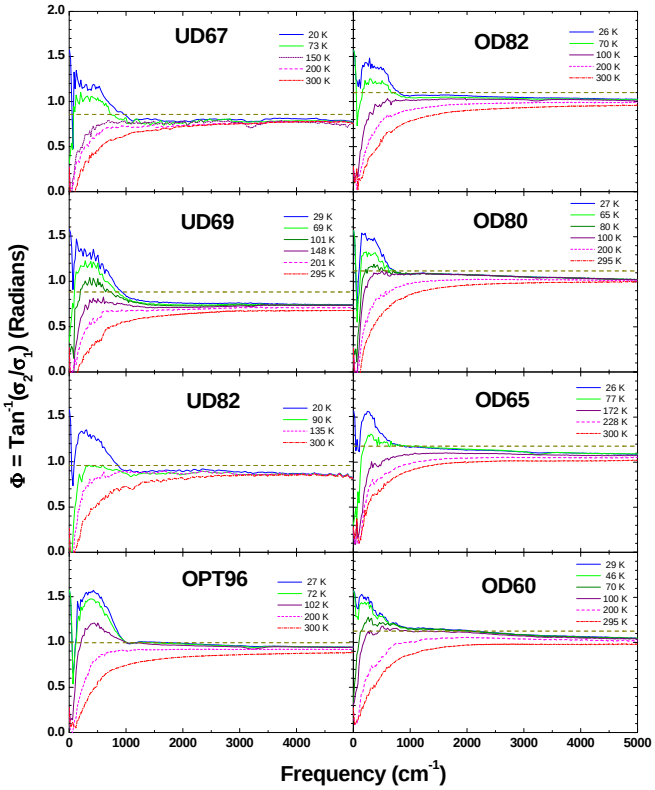


**Figure 4.** Phase of the optical conductivity, $\Phi(\omega) \equiv \tan^{-1}(\sigma_2(\omega)/\sigma_1(\omega))$ [78]. The dashed horizontal lines are obtained from the fitted straight lines in Fig. 3.

at various temperatures on a log-log scale. The dashed lines are linear least squares fits of the amplitude between 500 $cm^{-1}$ and 5000 $cm^{-1}$ in the normal state where the quantity $|\sigma(\omega)|$ shows negligible temperature dependence. The absolute value of the slope $(\gamma - 2)$ of the fitted straight line increases as the doping level increases. From the slope we can obtain the doping dependence of $\gamma(p)$, which decreases monotonically from 1.45 to 1.25 as doping increases (see figure 5).

In figure 4 we show the phase, $\Phi(\omega)$, of the optical conductivity for all our samples. We note that the phase is almost frequency independent over a wide spectral range above 1000 $cm^{-1}$ at all measured temperatures. The dashed horizontal line is the corresponding phase of the straight line fit of the amplitude (see figure 3). We observe that the van der Marel behavior holds over a wide spectral range, roughly between 500 $cm^{-1}$ and near 5000 $cm^{-1}$, at various temperatures, and over a wide rage of doping. We also note that at low frequencies, below 500 $cm^{-1}$, the optical conductivity shows a strong temperature dependence and deviates markedly from a constant. In figure 5 we plot the doping dependent exponent, $\gamma(p)$, which is extracted from the linear fits in figure 3. The exponent decreases monotonically as the doping increases. The dot-dashed line is a list squares fit of a straight line to the data. The lower dashed line is a predicted variation of this quantity with doping from a recent paper by Anderson[79].

In figure 6 we demonstrate how the value $\epsilon_H$ affects the amplitude and the phase

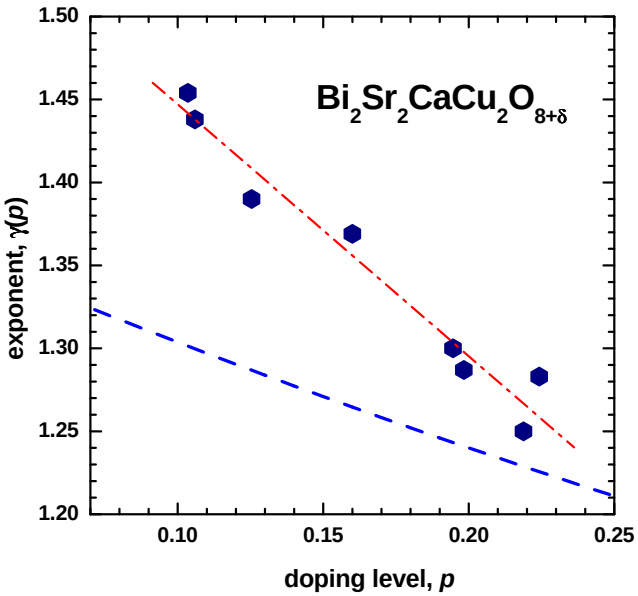


**Figure 5.** Doping dependent exponent, $\gamma(p)$. See the text for a detail description of the quantity $\gamma(p)$. The dashed line is a theoretical estimate of the variation of $\gamma(p)$ with doping due to Anderson, ref. [79]

**Table 1.** Doping levels ($p$), the background dielectric constant ($\epsilon_H$), and the plasma frequency ($\omega_p$) of our eight Bi-2212 samples.

| Samples | $T_c(K)$ | Doping level,$p$ | $\epsilon_H$ | $\omega_p$ (cm$^{-1}$) |
|---|---|---|---|---|
| UD67 | 67 | 0.103 | 3.14 | 15 050 |
| UD69 | 69 | 0.106 | 3.15 | 15 150 |
| UD82 | 82 | 0.125 | 3.21 | 16 300 |
| OPT96 | 96 | 0.160 | 3.52 | 17 000 |
| OD82 | 82 | 0.195 | 4.14 | 18 800 |
| OD80 | 80 | 0.198 | 4.15 | 18 700 |
| OD65 | 65 | 0.219 | 4.25 | 19 200 |
| OD60 | 60 | 0.224 | 4.19 | 18 900 |

of the optical conductivity. Note that $\epsilon_H$ affects only the imaginary part of the optical conductivity, $\sigma_2$. To see the effect we chose the data for optimally doped Bi-2212 at $T$=102 K and calculate the complex optical conductivity for four different values of $\epsilon_H$ between 2.50 and 6.00. It is clear from the figure that there is no significant effect below 1000 cm$^{-1}$ but the effect builds up rapidly as the frequency increases. In the upper panel we show calculated amplitudes on a log-log scale. As $\epsilon_H$ increases the absolute value of the slope in the amplitude between 500 and 5000 cm$^{-1}$ decreases. When $\epsilon_H$=3.52, the value we used in our analysis, the amplitude is the straightest over a wide range of frequencies. In the lower panel we show corresponding phases. As $\epsilon_H$ increases the slope in the phase changes from negative to positive. When $\epsilon_H$=3.52 the phase is almost frequency independent, i.e. the slope is zero. However to reach a definite conclusion from this type of analysis [78] one needs a model-independent way of estimating $\epsilon_H$.

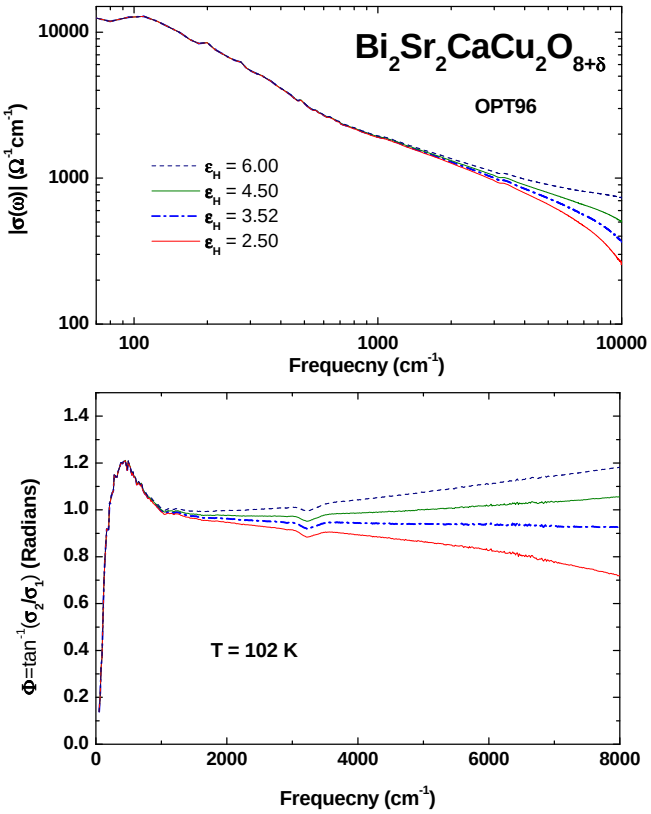


**Figure 6.** The effect of choosing different values of $\epsilon_H$ on the amplitude a) and the phase b) of the optical conductivity. Note that $\sigma_1$ is independent of $\epsilon_H$.

In figure 7 we show the temperature dependence of the dc resistivity of our eight Bi-2212 samples obtained from extrapolations to zero frequency of the normal state optical conductivities. These optically determined resistivities show the same features and trends that are seen with four-probe dc measurements. Starting with the optimally doped sample OPT96 we see the familiar linear variation of resistivity with temperature with a zero temperature intercept that is very close to the zero of the temperature axis. From the beginning of the study of the cuprates this behavior has been taken as evidence of an exotic transport mechanism. Interaction with a bosonic mode would also be linear with temperature in this range but would yield an intercept at approximately $\hbar\omega/4$ where $\omega$ is the frequency of the mode. For phonon modes involving oxygens this intercept would be at 100 K. Moving to underdoped samples we do find a higher intercept associated with the temperature dependence below about 150 K. Above this temperature the temperature dependence is similar to that of the optimally doped sample with a lower intercept on the temperature axis. The overdoped samples on the other hand show a more metallic temperature dependence with an upward curvature with the power law index of 1.64 for our most overdoped sample smaller than the $T^2$ expected for a Fermi liquid. These observations are consistent all previous systematic measurements of the dc resistivity [80, 81]. The message from the underdoped samples is that any bosonic spectral function causing this scattering has a temperature dependent amplitude with

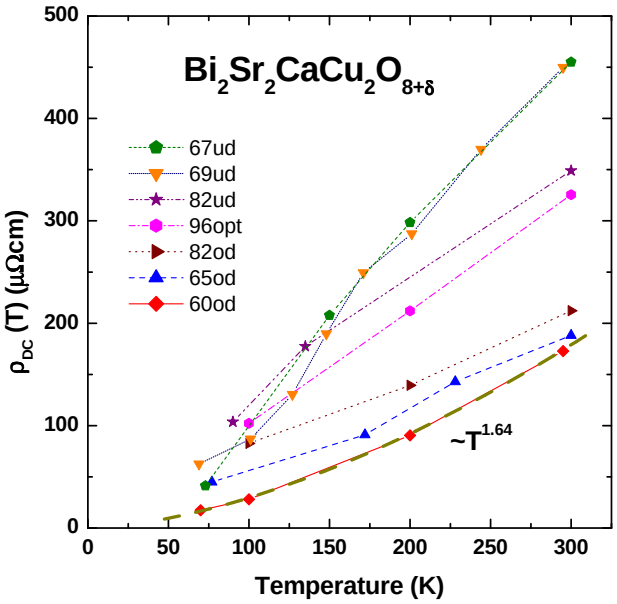


**Figure 7.** dc resistivity, $\rho_{dc}(T)$, extracted from low frequency extrapolations of normal state optical conductivities. The dashed curve through data points of our most overdoped sample is a fitted curve, $\rho_{DC}(T) = 0.0155\,T^{1.64}$. See the text for a detailed description of the extrapolation.

rapid changes occurring in the 150 K temperature range. This is in agreement with our study of another underdoped system Ortho II YBCO cite [48].

## 4. FGT sum rule, superfluid density and kinetic energy

Of the various techniques used to determine the superfluid density optics has the advantage that it gives the absolute value and in an anisotropic system, such as the high temperature cuprates, all the orthogonal components if an oriented crystal is used. However there are problems that make an accurate determination of the absolute magnitude difficult. The first of these is a need to determine accurately the reflectance in the low frequency region where the it approaches unity and where measurements on small crystals are difficult as the wavelength of the radiation used approaches the size of the samples.

Another source of uncertainty is the presence of a residual metallic conductivity in the superconducting state seen in many samples. This effect can be recognized by a downturn in reflectance at low frequency by as much as one to two percent. The resulting conductivity shows a peak removed from zero frequency characteristic of a disordered metallic material. [82] This low frequency suppression of reflectance is directly related to a sizable low frequency spectral weight in the optical conductivity and might cause some uncertainty in the estimated superfluid density. Here we try to minimize this uncertainty by estimating the super fluid density with the same criteria for all our Bi-2212 samples using the same experimental instrument and technique, the same method

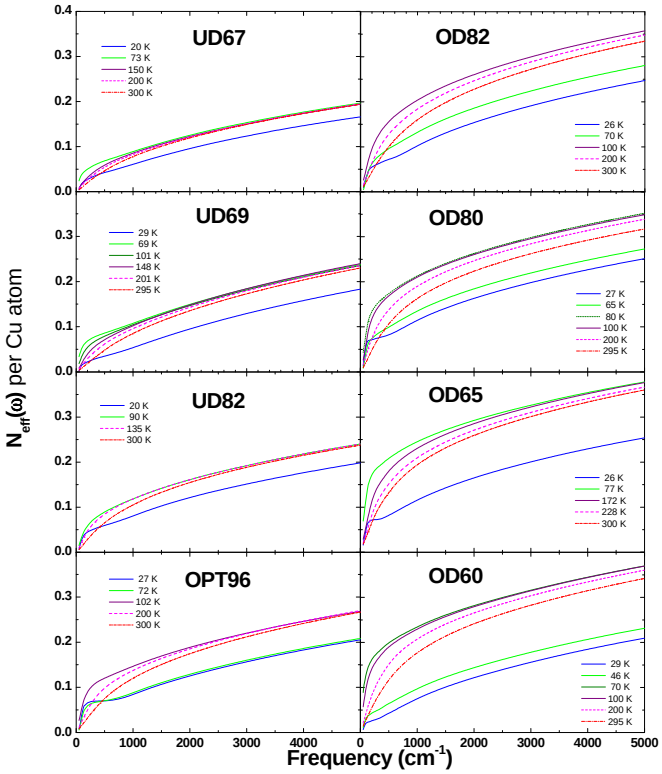


**Figure 8.** Frequency dependent spectral weight expressed as the number of effective charge carriers per Cu atom of Bi-2212, as is defined in Eg. 7.

of analysis, and the same low frequency cutoff of reflectance data, 50 $cm^{-1}$. With eight different data sets of the optical conductivity of Bi-2212, we obtain doping dependent superfluid density from the highly underdoped region to the overdoped region.

Figure 8 shows the frequency dependent accumulated spectral weight or the effective number of charge carriers per Cu atom of eight Bi-2212 samples at various temperatures below and above $T_c$. Overall, the spectral weight increases as we add carriers by doping as we expect. In the normal state, as the doping level increases the temperature dependent region in the spectral weight extends to higher frequency. As the temperature is lowered spectral weight is shifted to low frequency because of the narrowing of the Drude band.

Above 2000 $cm^{-1}$ the highest spectral weight curves are almost parallel to the curve in the superconducting state. The difference between the two parallel spectral weight curves gives us a rough estimate of the number of superfluid charge carriers per Cu atom, the superfluid density. This difference increases as the doping level increases; the higher the doping level, the higher is the superfluid density (see figure 11). The flat region spectral weight in the superconducting state is related to the dip below 1000 $cm^{-1}$ in the optical conductivity. We analyze spectral weight variations in detail using the optical sum rule [69, 74] with or without including the temperature dependence in the spectral weight.

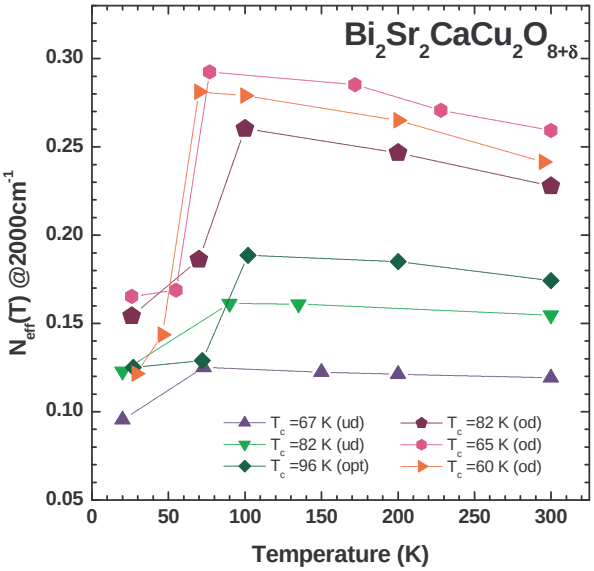


**Figure 9.** Temperature dependent spectral weight below2000 $cm^{-1}$ for six representative Bi-2212 samples. At this cutoff frequency the spectral weight increases as the temperature is lowered to drop rapidly at $T_c$ as the superconducting condensate forms. There is a monotonic increase of spectral weight with doping.

We describe next the method we use to obtain the superfluid density from the optical conductivity in the superconducting state. In the superconducting state we have two separate contributions to the real part of the optical conductivity: a delta function at the origin from the superconducting condensate and a regular non-superconducting part.

$$\sigma_1(\omega) = \sigma_{1s}\delta(0) + \sigma_1^{'}(\omega) \tag{8}$$

where $\sigma_{1s}$ is a contribution from the superfluid charge carriers and $\sigma_1^{'}(\omega)$ is a regular non-superconducting part of the optical conductivity. From the optical sum rule, we can describe the superfluid plasma frequency, $\omega_{ps}$ in terms of $\sigma_{1s}$; $\sigma_{1s} = \omega_{ps}^2/8$. Note that dimension of $\sigma_{1s}$ is frequency squared. The Kramers-Kronig (KK) transformation of the real part gives us the imaginary part, which also consist of two terms, as follows:

$$\sigma_2(\omega) \equiv \sigma_{2s}(\omega) + \sigma_2^{'}(\omega) \tag{9}$$

$$= \frac{2\sigma_{1s}}{\pi\omega} + \sigma_2^{'}(\omega) \tag{10}$$

where $\sigma_{2s}(\omega)$ is the imaginary part of the condensate conductivity and $\sigma_2^{'}(\omega)$ the imaginary part of the regular non superconducting part. The latter makes a KK pair with $\sigma_1^{'}(\omega)$.

Using KK transformations we can calculate $\sigma_2^{'}$ from $\sigma_1^{'}$, which is simply the optical conductivity in the superconducting state because $\sigma_{1s}$ is a delta function at zero frequency and is not seen at finite frequencies. We have already extracted the total $\sigma_2$ from the measured reflectance and a given $\epsilon_H$ by using KK analysis as described previously. So we can obtain $\sigma_{2s}$ by subtracting $\sigma_2^{'}$ from $\sigma_2$. Finally, we can calculate

the superfluid plasma frequency, which is closely related to the superfluid density, $N_s$, by the following equation:

$$\sigma_{2s}(\omega)\cdot\omega = \frac{2\sigma_{1s}}{\pi} = \frac{\omega_{ps}^2}{4\pi} = \frac{N_s e^2}{mV_{Cu}} \tag{11}$$

where $V_{Cu}$ is the volume per Cu atom, $e$ is the charge of an electron, and $m$ is the mass of a free electron.

After some units conversions, we get the following practical formula for the superfluid density, $N_s$.

$$N_s \cong 6.29\times10^{-10} V_{Cu}\cdot\sigma_{2s}(\omega)\cdot\omega \tag{12}$$

where $V_{Cu}$ is in $\mathring{A}^3$, $\sigma_{2s}$ in $\Omega^{-1}\mathrm{cm}^{-1}$, and $\omega$ in $\mathrm{cm}^{-1}$. For Bi-2212 $V_{Cu}$ is 112.6 $\mathring{A}^3$, which does not change much with doping.

Another independent method that yields the superfluid density from the optical conductivity is directly related to the 'missing spectral weight' in the optical conductivity when charge carries are paired and condense to form the superfluid. There is a fundamental difference between this and the previous method. For this method we need to have two optical conductivities (one in normal state and the other in superconducting state) while only one optical conductivity in the superconducting state is needed for the application of the previous method. We should note that the temperatures of the normal and superconducting states are not the same. The temperature difference may cause an unwanted error in the superfluid density extracted using this methods because the normal state spectral weight shows a temperature dependence (see figure 9) [48, 83] which will extend below the superfluid transition temperature. This method originates in the Ferrel-Glover-Tinkham (FGT) sum rule [14] which states that all the spectral weight lost at finate frequencies is transferred to the superconducting condensate delta function at zero frequency. In the formalism we can describe the superfluid plasma frequency in convenient units as follows:

$$\omega_{ps,sum}^2(\omega) = \frac{120}{\pi}\int_{0^+}^{\omega}[\sigma_{1,n}(\omega') - \sigma_{1,s}(\omega')]d\omega' \tag{13}$$

$$N_{s,sum}(\omega) \cong 4.26\times10^{-10}\cdot V_{Cu}\int_0^{\omega}(\sigma_{1,n}-\sigma_{1,s})d\omega'$$

where $\sigma_{1,n}$ and $\sigma_{1,s}$ are the real part of the optical conductivity of normal and superconducting states, respectively. $V_{Cu}$ is in $\mathring{A}^3$ and $\sigma_1$'s are in $\Omega^{-1}\mathrm{cm}^{-1}$. All frequencies are in $\mathrm{cm}^{-1}$ including $\omega_{ps,sum}$.

In conventional superconductors, where the pairing and the condensation are driven by potential energy, the FGT sum rule holds exactly. However, as Hirsch has proposed, the FGT sum rule can be violated in unconventional superconductors including the cuprates [15] and a modified FGT sum rule can be introduced with an extra kinetic energy terms as follows [16, 84]:

$$\omega_{ps}^2(\omega) = \frac{120}{\pi}\int_{0^+}^{\omega}\Delta\sigma_1(\omega')d\omega' + \frac{e^2ab}{\pi\hbar^2c^2V_{Cu}}\Delta E_{Kin}(\omega)$$

or

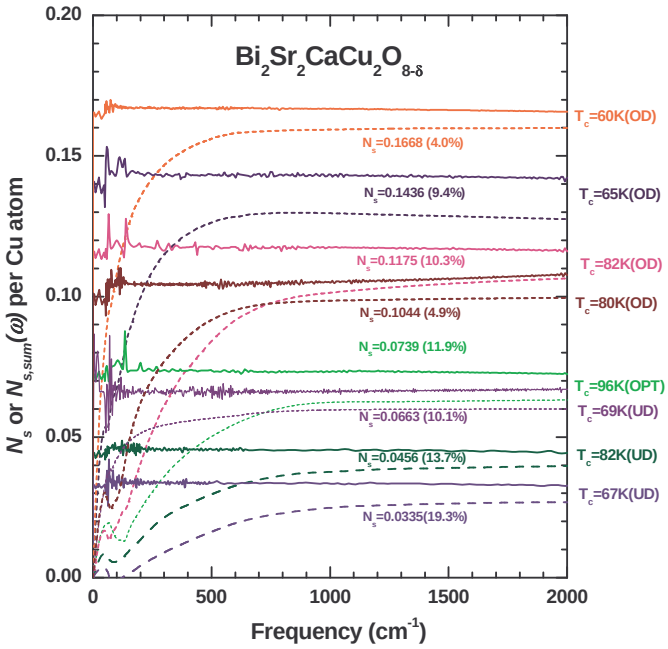


**Figure 10.** Superfluid densities obtained by two different methods using $\sigma_2(\omega)$ (Eq. 12) (solid curves) and using the FGT sum rule (Eq. 13) (dashed curves). See table 2 for detailed values of $N_s$.

$$\Delta E_{Kin}(\omega) = \frac{\hbar^2}{mab}[N_s - N_{s,sum}(\omega)] \tag{14}$$

or

$$\Delta E_{Kin}(\omega) \cong 0.261 \times [N_s - N_{s,sum}(\omega)] \ \text{(in eV)} \tag{15}$$

where $\Delta\sigma_1(\omega') = \sigma_{1,n}(\omega') - \sigma_{1,s}(\omega')$, $a$ and $b$ are the lattice constants of the ab-plane, $c$ is the speed of light, and $\Delta E_{Kin}(\omega)$ is the kinetic energy change when the system becomes a superconductor, i.e. $\Delta E_{Kin}(\omega) \equiv E^s_{Kin}(\omega) - E^n_{Kin}(\omega)$, where $E^s_{Kin}(\omega)$ and $E^n_{Kin}(\omega)$ are kinetic energy of the superconducting and the normal states, respectively. Note that Eq. 15 holds only for Bi-2212 systems.

In figure 9 we display a temperature dependent $N_{eff}(T)$ of our six representative Bi-2212 samples with a cutoff frequency of 2000 cm$^{-1}$. Above $T_c$ as the temperature decreases $N_{eff}$ increases almost linearly and the rate of increase grows as the doping level increases. We take into account this linear temperature dependence of $N_{eff}$ when we adjust the superfluid density, $N_{s,sum}$ (see figure 12) to obtain the kinetic energy change. We should note here that the temperature dependence of $N_{eff}$ depends on the cutoff frequency and doping level as well. Ortolani *et al.* have observed roughly $T^2$ dependence of $N_{eff}$ in $La_{2-x}Sr_xCuO_4$ (LSCO) systems [83].

In figure 10 we show the superfluid densities obtained from the two different methods, i.e. using Eq. 12 and Eq. 13. Here we do not include the temperature dependence of $N_{eff}$ to obtain $N_{s,sum}(\omega)$ yet. In principle, $N_s(\omega)$ is frequency independent and $N_{s,sum}(\omega)$ approaches a saturation value as the frequency increases. We

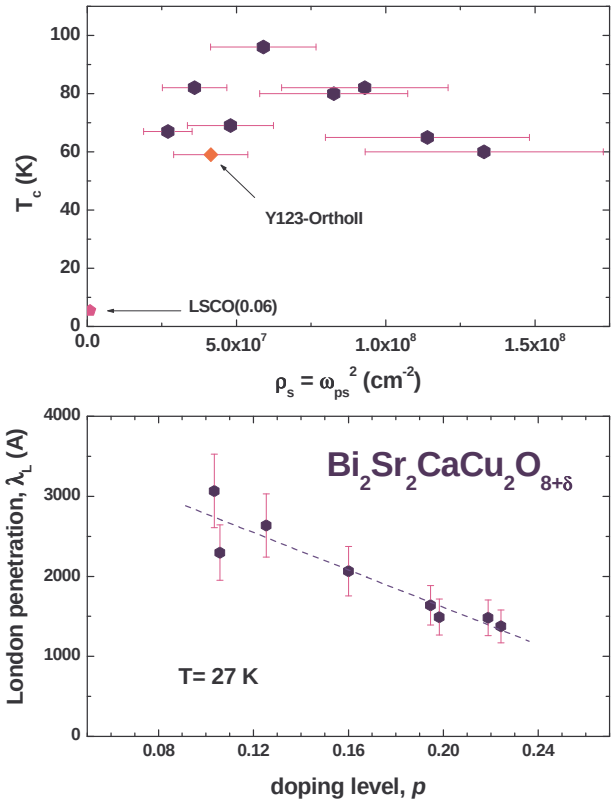


**Figure 11.** In the upper panel we display $T_c$ versus $\rho_s \equiv \omega_{ps}^2$. We added two data point from underdoped LSCO with $T_c$= 5.5 K and underdoped Y123 in the orthoII phase with $T_c$= 59 K. In the lower panel we display doping dependent London penetration depth, $\lambda_L(p)$.

**Table 2.** Superfluid densities of our eight Bi-2212 samples. $N_s$ are the extracted superfluid densities using Eq. 12 and $N_{s,sum}$ are the extracted superfluid densities using FGT sum rule, Eq. 13, integrated up to 2000 cm$^{-1}$. $N_{s,diff}(\%)$ are the percentage differences between superfluid densities determined by the two methods (see in the text for a more detailed description).

| Samples | $T_c(K)$ | $p$ | $N_s$ | $N_{s,sum}$ | $N_{s,diff}(\%)$ |
|---|---|---|---|---|---|
| UD67 | 67 | 0.103 | 0.0335 | 0.0270 | 19.3 |
| UD69 | 69 | 0.106 | 0.0663 | 0.0596 | 10.1 |
| UD82 | 82 | 0.125 | 0.0456 | 0.0394 | 13.7 |
| OPT96 | 96 | 0.160 | 0.0739 | 0.0651 | 11.9 |
| OD82 | 82 | 0.195 | 0.1044 | 0.0993 | 4.9 |
| OD80 | 80 | 0.198 | 0.1175 | 0.1054 | 10.3 |
| OD65 | 65 | 0.219 | 0.1436 | 0.1301 | 9.4 |
| OD60 | 60 | 0.224 | 0.1668 | 0.1601 | 4.0 |

observe that $N_{s,sum}$ saturates more quickly as doping increases, which is consistent with the observation of Homes *el al.* [85] in the $YBa_2Cu_3O_{6+x}$ (Y123) system except that our saturation frequency is lower than what they observed. The number in the parenthesis is a percentage difference between $N_s$ and the saturated $N_{s,sum}$, i.e. $(N_s - N_{s,sum})/N_s \times 100$.

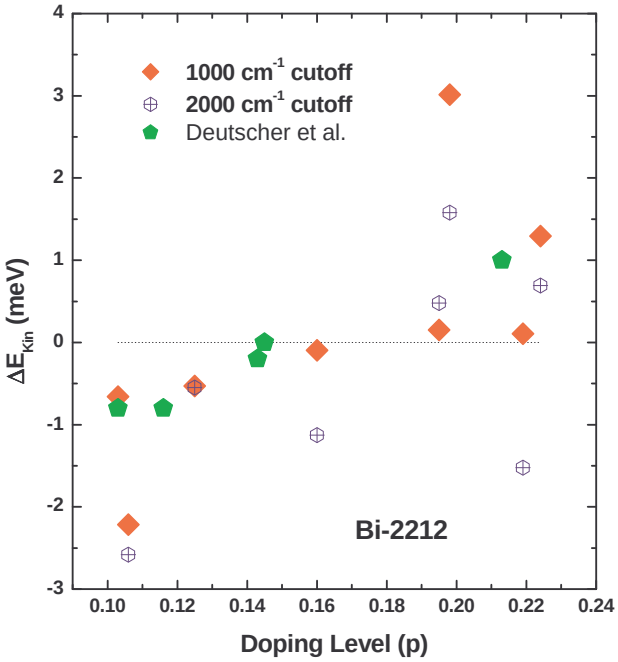


**Figure 12.** Doping dependent kinetic energy change, $\Delta E_{Kin} \equiv E^s_{Kin} - E^n_{Kin}$, of Bi-2212 when the system becomes superconductor. We also show data points from Deutscher *et al.* of Bi-2212 systems [17]

Roughly, we observe that the superfluid density increases as doping increases. Through the whole spectral range and at all doping levels the saturated $N_{s,sum}$ is smaller than $N_s$ and the FGT sum rule is violated. However, when we take into account the temperature dependence for $N_{s,sum}$, $N_{s,sum}$ is smaller than $N_s$ in underdoped region and is larger than $N_s$ in overdoped (see figure 12). In other words the sumrule violation changes sign at this doping level.

In the upper panel of figure 11 we show a $T_c$ versus $\rho_s \equiv \omega^2_{ps}$ graph. We do not observe so-called "boomerang" effect [86, 87] where at higher doping levels the superfluid density decreses. Also we add two additional data points for 6 % Sr doped LSCO ($T_c$=5.5K) and a well-ordered underdoped Y123-OrthoII ($T_c$=59 K) [48]. In the lower panel we show the doping dependent London penetration depth, $\lambda_L(p) \equiv 1/(2\pi\omega_{ps})$ where $\omega_{ps}$ is in cm$^{-1}$ units. As doping increases the London penetration depth decreases monotonically with values ranging between 1000 and 3000 Å.

In figure 12 we show the doping dependent kinetic energy change, $\Delta E_{Kin}(p)$, of Bi-2212 samples with two different cutoff frequencies; 1000 and 2000 cm$^{-1}$. When calculating $\Delta E_{Kin}(p)$ we take into account the temperature dependent spectral weight (see Fig. 9) of the normal state i.e. we extrapolate the temperature dependent trend to get an appropriate normal state $N_{eff}$ at the temperature of the superconducting state considered. Even though the data points do not show a very smooth doping dependence we can clearly observe a crossover from negative (underdoped) to positive (overdoped) kinetic energy change, which is consistent with the result of Deutscher *et al.* [17] in the same Bi-2212 system. Their data are also shown in the figure.

## 5. The extended Drude model and the optical self-energy

The extended Drude model offers a detailed description of the charge carrier scattering spectrum and its contribution to the effective mass [29, 88]. In this picture the elastic scattering rate in the Drude expression is allowed to have a frequency dependence and an extra real quantity, $\omega\lambda(\omega)$ is added to the (imaginary) scattering rate. This is necessary to retain the Kramers-Kronig relation between $\sigma_1(\omega)$ and $\sigma_2(\omega)$. In this formalism we can introduce an interesting and useful quantity, the optical self-energy, $\Sigma^{op}(\omega)$, which is closely related to the quasiparticle self-energy [8, 89].

$$\begin{aligned}\sigma(\omega,T) &= i\frac{\omega_p^2}{4\pi}\frac{1}{\omega+[\omega\lambda(\omega,T)+i1/\tau(\omega,T)]} \\ &= i\frac{\omega_p^2}{4\pi}\frac{1}{\omega-2\Sigma^{op}(\omega,T)}\end{aligned} \tag{16}$$

where $\omega_p$ is the plasma frequency, $1/\tau(\omega,T)$ is the optical scattering rate, and $\lambda(\omega)+1 \equiv m^*(\omega)/m$, $m^*(\omega)$ is an effective mass and $m$ is the bare mass. The optical self-energy is a complex function, $\Sigma^{op}(\omega,T) \equiv \Sigma_1^{op}(\omega,T)+i\Sigma_2^{op}(\omega,T)$, where $-2\Sigma_1^{op}(\omega,T) = \omega\lambda(\omega,T)$ and $-2\Sigma_2^{op}(\omega,T) = 1/\tau(\omega,T)$. $\Sigma_1^{op}$ and $\Sigma_2^{op}$ make a Kramers Kronig pair. The optical self-energy contains the plasma frequency, which includes the spectral weight of the free carrier part of the optical conductivity. We obtained the plasma frequency by using a procedure introduced in a previous study [68]. The plasma frequencies are displayed in table 1. The optical self-energy at high frequencies depends strongly on $\epsilon_H$ (see figure 6 and its caption). The optical self-energy is, apart from a $(cos\theta - 1)$ factor where $\theta$ is a scattering angle, an average over the Fermi surface of the quasiparticle self-energy [7, 8, 90, 91] as measured by angle resolved photoemission spectroscopy (ARPES). ARPES has a capability of k-space resolution while optics has the advantage of better overall energy resolution. The self-energies measured by the two spectroscopy techniques (optical and ARPES) show qualitatively the same properties [8, 30, 34]. However, on a quantitative level there are some fundamental differences between them [89].

Figure 13 displays the optical scattering rates of our eight Bi-2212 samples at various temperatures above and below $T_c$. At room temperature the overall scattering rate decreases as the doping increases. The scattering rate is a fairly linear as a function of frequency and the slope decreases monotonically with the doping. This linear dependency was described by the phenomenological marginal Fermi liquid theory [57]. We do not observe any hints of "the plateau" in the scattering of any of our samples up to 8000 $cm^{-1}$, as suggested by van der Marel *et al.* [78]. At lower temperatures a sharp step-like feature appears in the spectrum. The onset temperature of this feature is higher than $T_c$ for underdoped samples and $\cong T_c$ for optimally and overdoped samples. This feature can be fitted with a formalism [48, 92], based on a method proposed by Shulga *et al.* [93]. For the fit we need two separate bosonic scattering channels; one is scattering by a sharp mode and the other a broad background. Hwang *et al.* showed

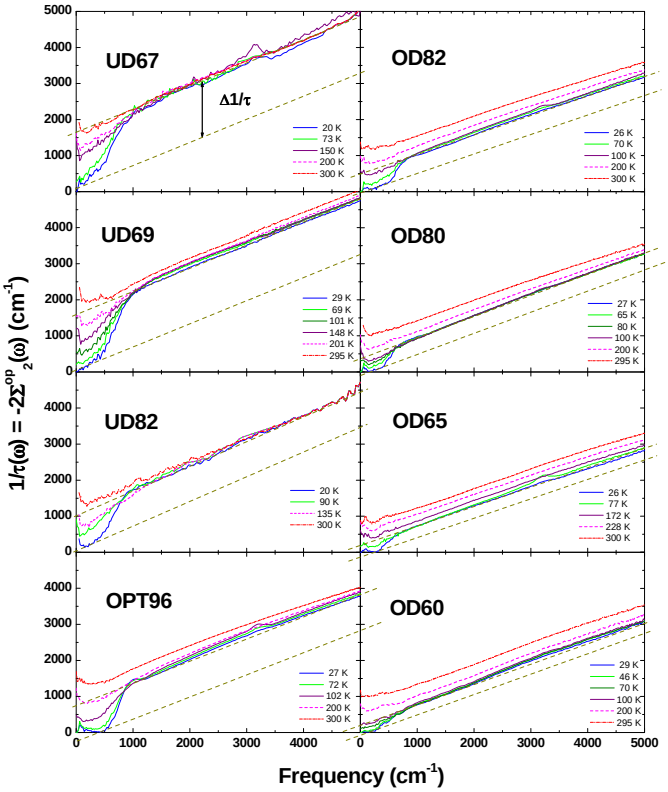


**Figure 13.** The optical scattering rate or the imaginary part of the optical self-energy of ab-plane Bi-2212 at various doping levels and temperatures. $\Delta 1/\tau$ can be a measure of intensity of the step-like feature, which is correlated to the magnetic resonance mode [8, 30, 48]. The intensity of the step shows strong temperature and doping dependencies.

that the step-like feature and the sub-linear part of high frequency scattering rate were attributed to the sharp mode and the broad background in the spectral function $\alpha^2F(\Omega)$, respectively [48]. In the superconducting state we need a formalism that incorporates the superconducting gap and coherence factors. Qualitatively a similar picture was derived and applied to optimally doped Bi-2212 system by Schachinger *et al.* [90]. We estimate the contribution of the sharp mode to the optical scattering rate by the height of the step in the scattering rate, which is proportional to the area under the mode in the spectral function. We measure the height of the step as follows [8]: we draw a dashed line parallel to the high frequency sub-linear trend from an onset point of substantial scattering. The difference between this line and the actual high frequency scattering, $\Delta 1/\tau$ (shown in the figure 13), is our estimate of the contribution of the sharp mode to the optical scattering. A doping dependent step intensity, $\Delta 1/\tau(p)$, is shown in figure 14. In the figure we also show a normalized scattering rate, $(\Delta/\tau)/(1/\tau@5000\text{cm}^{-1})$, divided by the value at 5000 $\text{cm}^{-1}$. The step in intensity decreases rapidly as the doping level increases and becomes zero near doping a level of $p \sim 0.24$ within the superconducting dome, where the superconductivity is still strong in terms of $T_c \sim 55$ K.

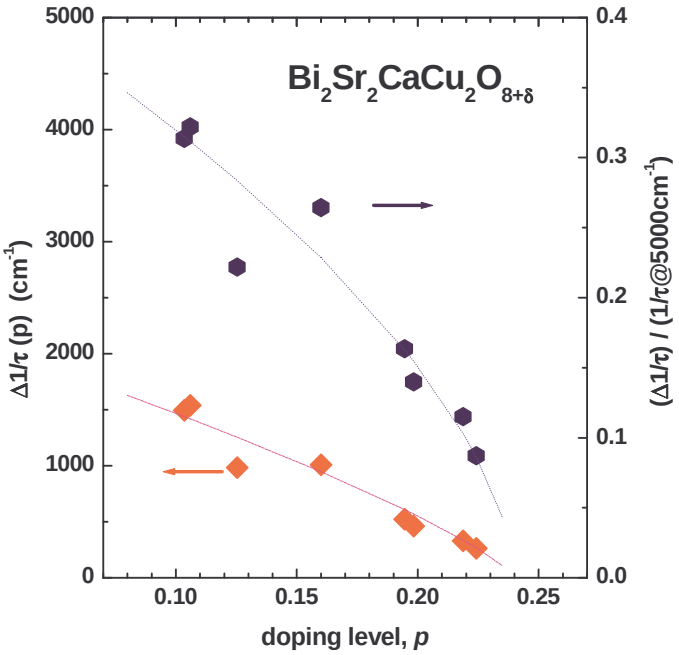


**Figure 14.** The doping dependent intensity of the step-like feature in the optical scattering rate.

In figure 15 we display the real part of the optical self-energy of Bi-2212. This quantity and the scattering rate make a KK pair. At room temperature we see only a very broad background spectrum. The peak frequency of the broad background increases as the doping increases. As the temperature is lowered a well-defined sharp peak appears out of the broad room temperature background with the same onset temperature as the step-like feature in the scattering rate and the peak grows as the temperature is reduced further. Johnson *et al.* have also resolved a sharp peak and a broad background in ARPES quasiparticle self-energy spectra in the ($\pi$,$\pi$) direction of Bi-2212 systems and correlated the sharp mode to the magnetic resonance mode of inelastic neutron scattering [37]. More recently similar conclusions have been reached by Kordyuk *et al.* [42]. The optical self-energy and ARPES quasiparticle self-energy show strong similarity in terms of their shapes and temperature and doping dependencies [8]. Both self-energies have a sharp mode and a broad background at low temperature below $T_c$ while optics shows much better energy resolution. The mode frequencies from both techniques have an interesting relation: $\Omega_{optical} \cong \sqrt{2}\ \ \Omega_{ARPES}$, where $\Omega_{optical}$ and $\Omega_{ARPES}$ are the optical and ARPES mode frequencies, respectively. The relation is consistent with a theoretical prediction [89]. Furthermore Hwang *et al.* have analyzed temperature dependent intensity of the step-like feature in the optical scattering rate of Y123-OrthoII and found a direct correlation between the step feature in the scattering and the magnetic resonance mode of inelastic neutron scattering (INS) [48].

In the upper panel of figure 16 we show the sharp peak separated from the broad background in the real part of the optical self-energy and fitted it to a Lorentzian function to obtain the center frequency, the width, and the height of the peak and the

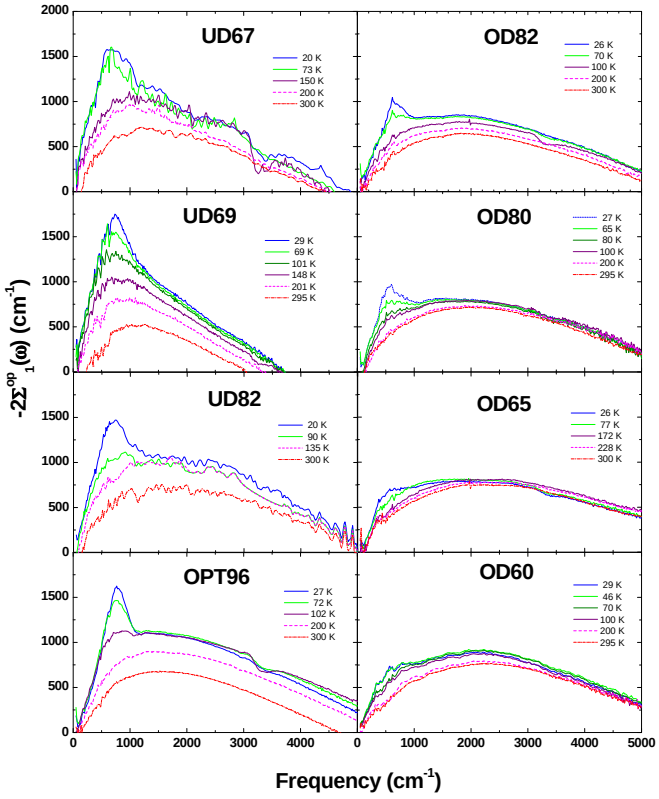


**Figure 15.** The real part of the optical self-energy of eight Bi-2212 samples at various temperatures. We are able to resolve a sharp peak and a broad background in the spectra. The sharp peak shows strong temperature and doping dependencies.

area under it. For the two most underdoped samples it is a little difficult to separate the peak from the broad background because the peak evolves gradually from the broad peak of the background. We display the doping dependent properties of the peak in the lower panel of the figure. The center frequency (the width) seems to be maximized (minimized) near the optimally doping level. Note that the width does not change much through a wide range of doping. The area and height show a strong doping dependence in the overdoped region; the intensities of both quantities decrease very rapidly as doping increases and finally become zero simultaneously within the superconducting dome with a hole doping level, $p \sim 0.24$ estimated from extrapolations. This result is consistent with the doping dependent intensity of the step-like feature in the scattering rate. In the same panel we show two data points (stars) extracted from the quasiparticle self-energy in a recent tunnelling study by Zasadzinski *et al.* [40, 94].

For another measure of the strength of the interaction of the charge carriers with the bosonic sharp mode we use the procedure introduced by Marsiglio *et al.*, Carbotte *et al.*, and Abanov *et al.* [30, 95, 96] where the bosonic spectral function, $W(\omega)$, is derived from the second derivative of the optical scattering rate times the frequency.

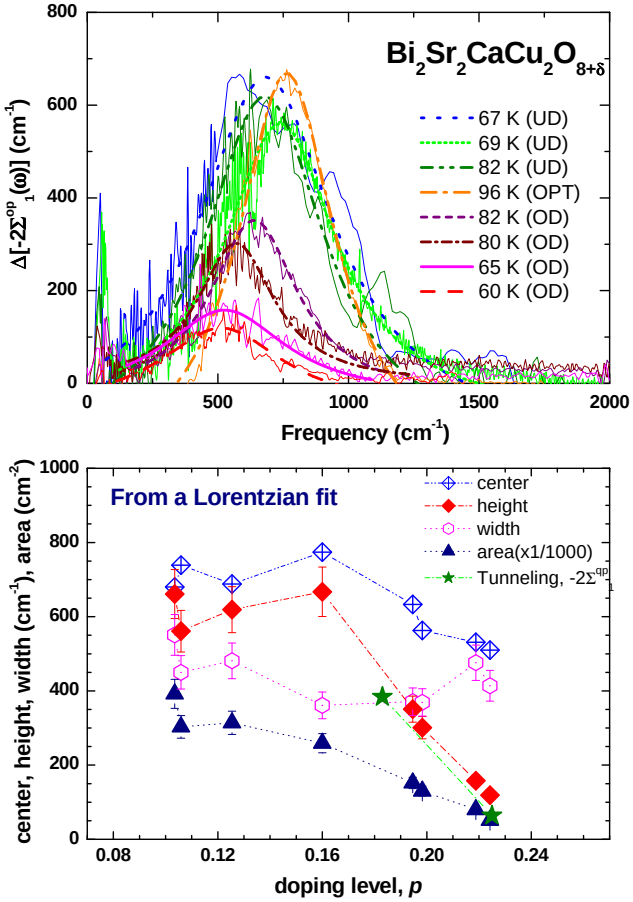


**Figure 16.** In the upper panel we show the sharp mode separated from the high temperature broad background in the real part of the self-energy and a Lorentzian fit for each doping level. In the lower panel we show the center frequency, the height, the width of the sharp mode and the area under the mode obtained from the Lorentzian fit. The two star symbols are extracted from the self-energy in a recent tunnelling study by Zasadzinski *el al.* [40, 94].

This function can be described as follows [32, 88, 95]:

$$W(\omega) \equiv \frac{1}{2\pi}\frac{d^2}{d\omega^2}\left[\frac{\omega}{\tau(\omega)}\right] \tag{17}$$

and $W(\omega) \approx \alpha^2 F(\omega)$ at zero temperature in the normal state, where $\alpha$ is a coupling constant, and $F(\omega)$ is a bosonic density of states. To obtain the spectral function ($W(\omega)$) we followed a smoothing procedure introduced by Tu *et al.* [32]. We fit $1/\tau(\omega)$ (see figure 13) with a polynomial with ten terms to catch the main frequency in the spectra without including too much experimental random-noise.

In the upper panel of figure 17 we show the bosonic spectral function obtained using the second derivative method, $W(\omega)$ for our six representative Bi-2212 samples at their lowest temperature. In the figure we have subtracted the room temperature background $W(\omega)$ from $W(\omega)$ at the lowest temperature. We should note that the bosonic mode is enhanced in the superconducting state. However, the qualitative doping dependent

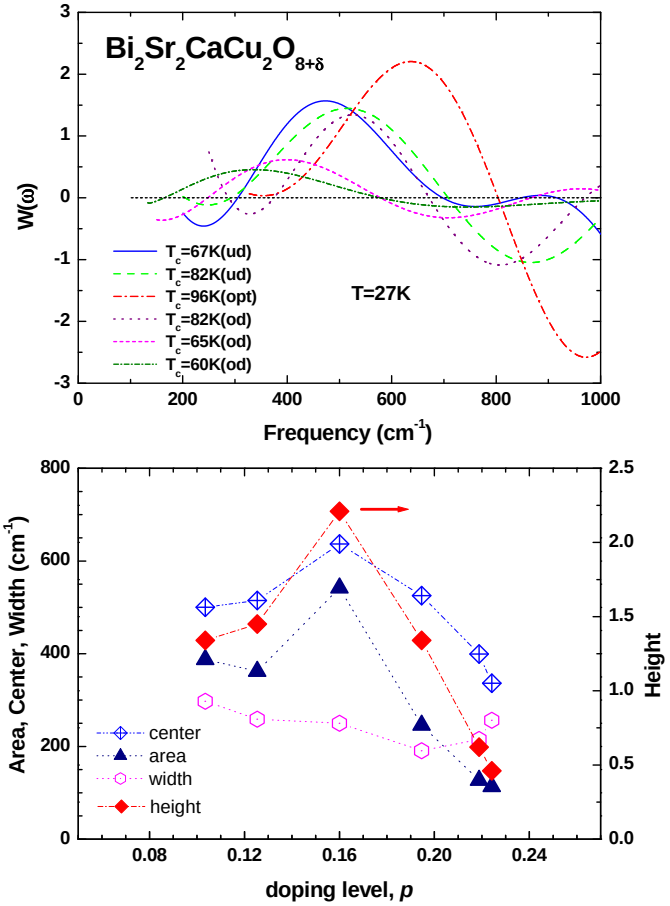


**Figure 17.** In the upper panel we show the bosonic spectral function, $W(\omega)$, obtained by using the second derivative formalism (see Eq. 17) at a superconducting state, $T \sim 27$ K. We observe sharp mode at low frequency range. In the lower panel we show the center frequency, the height, the width of the sharp mode and the area under the mode in $W(\omega)$.

trend is not affected by the gap [89]. In the lower panel of the figure we display the doping dependent properties of the peak: the center frequency, the width, and the height of the peak, and the area under the peak. The area is roughly proportional to the quantity, $\Delta 1/\tau$; it roughly follows the same doping dependent trend as $\Delta 1/\tau$. The extrapolation of the variation with doping of the height and area suggests that the mode will disappear within the superconducting dome in the Bi-2212 phase diagram. The polynomial fit method is fairly robust with respect to experimental noise. We compared this method with alternate methods including an inverse matrix method [97] and found that in the Ortho II material at least, this method gave a well ordered temperature sequence for both the peak position and frequency where alternate methods tended to scramble these quantities.

Since the mode disappears above a critical doping level in the phase diagram leaving the broad background as the only component in the interacting bosonic spectrum it is important to investigate this spectrum. We obtained the bosonic spectral functions

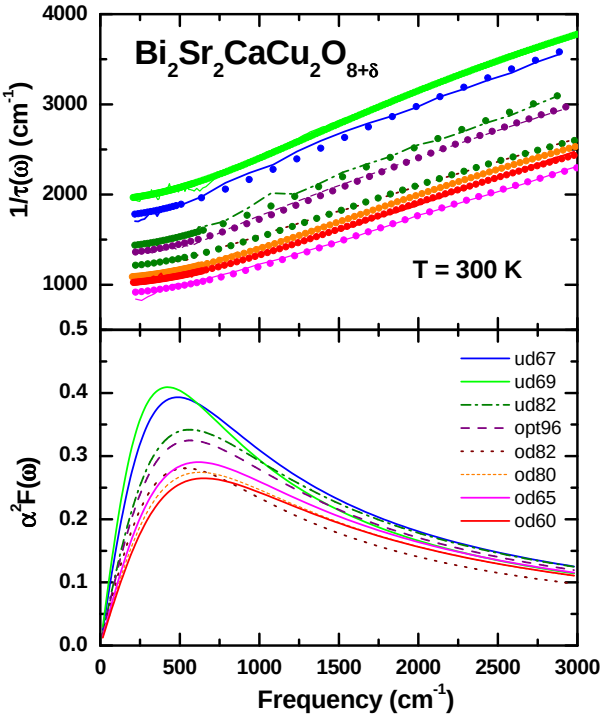


**Figure 18.** In the upper panel we show that the optical scattering rates (lines) of our eight Bi-2212 samples at room temperature and their fits (symbols) by using the methods introduced in a literatures [48, 92]. In the lower panel we display the MMP bosonic spectral function, $\alpha^2F(\omega)$, from the fits in the upper panel.

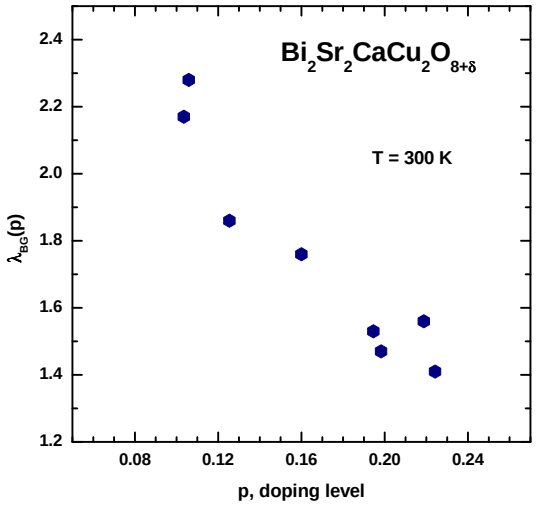


**Figure 19.** Doping dependent mass enhancement factor, $\lambda(p) = 2\int_0^{\omega_c} \alpha^2F(\omega')/\omega' d\omega'$, where $\omega_c$=3000 cm$^{-1}$, at room temperature. We used the extracted spectral function, $\alpha^2F(\omega)$, in the lower panel of figure 18 to get the coupling constant, $\lambda(p)$.

of our eight Bi-2212 samples by fitting the room temperature scattering rate with the Millis-Monien-Pines (MMP) type background [19] using the methods introduced by Sharapov *et al.* [48, 92]. In the upper panel of figure 18 we show the fits (symbols) and data (lines) of the optical scattering rate. In the lower panel of the figure we display the

corresponding bosonic spectral functions. The spectral function shows a slight doping dependence at low frequencies. As we move closer to the antiferromagnentic phase boundary the spectral function grows in strength and develops a more defined peak at low frequency. We also obtain the coupling constant, $\lambda$, for this spectrum, which is defined by $\lambda = \int_0^{\omega_c} \alpha^2 F(\omega')/\omega' d\omega'$ with $\omega_c = 3000\ \mathrm{cm}^{-1}$. The resulting doping dependent coupling constant, $\lambda_{BG}(p)$, is shown in Fig. 19. There is a strong doping dependence in the coupling constant, range from 2.3 to 1.4. The value decreases monotonically as doping level increases. This behavior is not consistent with an observation of Padilla *et al.* in LSCO systems [98] who suggest that there is little doping dependence of the carrier mass which is given by $m^* = m(1 + \lambda)$ across the phase diagram.

## 6. Discussion and conclusions

### *6.1. The superfluid density and the kinetic energy change*

The doping dependence of the superfluid density in the cuprates has been of great interest from early on when Uemura *et al.* found using muon scattering that the superfluid density increased with doping and was proportional to the superconducting transition temperature [99]. This so called Uemura relationship holds only up to the optimal doping level at which point as $T_c$ stops increasing while the superfluid density continues to increase. There have been reports for example by Niedermayer *et al.* who studied overdoped Tl-based ($Tl_2Ba_2CuO_{6+\delta}$: Tl-2201) cuprates by muon spin resonance of a so-called boomerang effect where the superfluid density *decreases* in the overdoped region as the doping level *increases* [86]. As we see in Fig. 11 our data, obtained by two different methods, shows that the superfluid density continues to increase in the overdoped region and there is no boomerang effect in this material.

In conventional superconductors the Ferrel-Glover-Tinkham (FGT) sum rule holds. However, the c-axis optical transport in the cuprates shows a strong violation of the FGT sum rule which has been attributed to a kinetic energy driven superconductivity [100]. Whether the FGT sum rule holds or not in ab-optical transport has been the subject of some controversy [101, 102, 103]. Here we find, as shown in Fig. 12, that a measurable FGT sum rule violation can be observed in ab-plane transport of Bi-2212. We do find that we have to take account the temperature dependence of the spectral weight and extrapolate it into the superconducting state. This result is consistent with Deutscher *et al.* [17].

### *6.2. The sharp mode and the broad background in the optical self-energy*

We have verified the behavior of the sharp mode observed by Hwang *et al.* [8] over a wide range of dopings with more samples which is shown in Fig. 14 and Fig. 16 and with a different method of analysis, the second derivative method, the result of which is shown in Fig. 17.

We also have studied the broad background in more detail; we extracted doping dependent bosonic spectra shown in Fig. 18 from room temperature optical scattering rates. The broad peak of the background moves to lower frequencies and its intensity increases as doping decreases, which is qualitatively consistent with Fig. 51 of Ref. [4]. The coupling constant of the room temperature background, $\lambda_{BG}(p)$, which is displayed in Fig. 19, decreases significantly as doping increases which agrees with previous studies [37, 68].

### *6.3. Summary and conclusion*

We obtained the superfluid density with two different methods from our ab-plane optical conductivity and observed that the superfluid density increased monotonically with hole doping level. The smooth and monotonic increase of superfluid density with doping supports an overall consistency of our study. We took into account the temperature dependence in the optical spectral weight to extracting the superfluid density and observed a violation of the FGT sumrule, the result of which causes a change of the kinetic energy of the charge carriers at the superconducting transiotion. Kinetic energy increases (decreases) in overdoped (underdoped) systems as the system becomes a superconductor. We also confirmed our previous work (Ref. [8]) with more samples and a different way of analysis. We resolved a sharp mode out of a broad background in the optical self-energy. The temperature and doping dependence of the sharp mode is dramatic; the onset temperature $T_s$ of the sharp mode is above (at) $T_c$ in underdoped (overdoped) systems and the intensity of the mode gets weakened strongly in the overdoped region with increasing doping and an extrapolation of the doping trend shows a complete disappearance above a critical doping, $p_c \sim 0.24$, within the superconducting dome. The broad background presents at all temperatures and doping levels and shows relatively weak doping and temperature dependence. However the coupling constant of the background decreases measurably as doping increases.

## Acknowledgments

This work has been supported by the Canadian Natural Science and Engineering Research Council and the Canadian Institute of Advanced Research. We thank H. Eisaki and M. Greven for supplying us with several crystals. Their work at Stanford University was supported by the Department of Energy's Office of Basic Sciences, Division of Materials Science. The work at Brookhaven was supported in part by the Department of Energy.

## References

[1] Bednorz T G and Müller K A 1986 *Z. Phys. B* **64** 189
[2] Carbotte J P 1990 *Rev. Mod. Phys.* **62** 1027

[3] McMillan W L and Rowell J M 1969 in *Superconductivity Vol 1* (ed. Parks R D) 561 (New York: Dekker)
[4] Eschrig M 2006 *Advances in Physics* **55** 47
[5] Damascelli A, Hussain Z and Shen Z -X 2003 *Rev. Mod. Phys.* **75** 473
[6] Mourachkine A 2005 *Modern Physics Letters B* **19** 743
[7] Kaminski A, Mesot J, Fretwell H, Campuzano J C, Norman M R, Randeria M, Ding H, Sato T, Takahashi T, Mochiku T, Kadowaki K and Hoechst H 2000 *Phys. Rev. Lett.* **84** 1788
[8] Hwang J, Timusk T and Gu G D 2004 *Nature (London)* **427** 714
[9] Basov D N and Timusk T 2005 *Rev. Mod. Phys.* **77** 721
[10] Puchkov A V, Fournier P, Basov D N, Timusk T, Kapitulnik A and Kolesnikov N N 1996 *Phys. Rev. Lett.* **77** 3212
[11] Puchkov A V, Basov D N and Timusk T 1996 *J. Physics: Condensed Matter* **8** 10049
[12] Quijada M A, Tanner D B, Kelley R J, Onellion M, Berger H and Margaritondo G 1999 *Phys. Rev. B* **60** 14917
[13] Liu H L, Quijada M A, Zibold A M, Yoon Y -D, Tanner D B, Cao G, Crow J E, Berger H, Margaritondo G, Forro L, Beom-Hoan O, Markert J T, Kelly R J and Onellion M 1999 *J. Physics: Condensed Matter* **11** 239
[14] Ferrell R A and Glover III R E 1956 *Phys. Rev.* **109** 1398; Glover III R E and Tinkham M 1956 *Phys. Rev.* **104** 844; 1957 *Phys. Rev.* **108** 243
[15] Hirsch J 1992 *Phsica C* **199** 305
[16] Hirsch J and Marsiglio F 2000 *Phys. Rev. B* **62** 15131
[17] Deutscher G, Santander-Syro A F and Bontemps N 2005 *Phys. Rev. B* **72** 092504
[18] Monthoux P, Balatsky A V and Pines D 1991 *Phys. Rev. Lett.* **67** 3448
[19] Millis A J, Monien H and Pines D 1990 *Phys. Rev. B* **42** 167
[20] Rossat-Mignod J, Regnault L P, Vettier C, Bourges P, Burlet P, Bossy J, Henry J Y and Lapertout G 1991 *Physica C* **185-189** 86
[21] Mook H A, Yethiraj M, Aeppli G, Mason T E and Armstrong T 1993 *Phys. Rev. Lett.* **70** 3490
[22] Fong H F, Keimer B, Anderson P W, Reznik D, Dogan F and Aksay I A 1995 *Phys. Rev. Lett.* **75** 316
[23] Mook H A, Dai P, Hayden S M, Aeppli G, Perring T G and Dogan F 1998 *Nature (London)* **395** 580
[24] Dai P, Mook H A, Hayden S M, Aeppli G, Perring T G, Hunt R D and Doan F 1999 *Science* **284** 1344
[25] Fong, H F, Bourges P, Sidis Y, Regnault L P, Ivanov A, Gu G D, Koshizuka N and Keimer B 1999 *Nature (London)* **398** 588
[26] He H, Sidis Y, Bourges P, Gu G D, Ivanov A, Koshizuka N, Liang B, Lin C T, Regnault L P, Schoenherr E and Keimer B 2001 *Phys. Rev. Lett.* **86** 1610
[27] He H, Bourges P, Sidis Y, Ulrich C, Regnault L P, Pailhes S, Berzigiarova N S, Kolesnikov N N and Keimer B 2002 *Science* **295** 1045
[28] Thomas G A, Orenstein J, Rapkine D H, Capizzi M, Millis A J, Bhatt R N, Schneemeyer L F and Waszczak J V 1988 *Phys. Rev. Lett.* **61** 1313
[29] Puchkov A V, Basov D N and Timusk T 1996 *J. Phys.: Condens. Matter* **8** 10049
[30] Carbotte J P, Schachinger E and Basov D N 1999 *Nature (London)* **401** 354
[31] Abanov Ar and Chubukov A V 1999 *Phys. Rev. Lett.* **83** 1652
[32] Tu J J, Homes C C, Gu G D, Basov D N and Strongin M, 2002 *Phys. Rev. B* **66** 144514
[33] Shen Z -X and Schrieffer J R 1997 *Phys. Rev. Lett.* **78** 1771
[34] Norman M R and Ding H 1998 *Phys. Rev. B* **57** R11089
[35] Campuzano J C, Ding H, Norman M R, Fretwell1 M H, Randeria M, Kaminski1 A, Mesot J, Takeuchi T, Sato T, Yokoya T, Takahashi T, Mochiku T, Kadowaki K, Guptasarma P, Hinks D G, Konstantinovic Z, Li Z Z0 and Raffy H 1999 *Phys. Rev. Lett.* **83** 3709
[36] Bogdanov P V, Lanzara A, Kellar S A, Zhou X J, Lu E D, Zheng W J, Gu G, Shimoyama J -I,

Kishio K, Ikeda H, Yoshizaki R, Hussain Z and Shen Z -X 2000 *Phys. Rev. Lett.* **85** 2581
[37] Johnson P D, Valla T, Fedorov A V, Yusof Z, Wells B O, Li Q, Moodenbaugh A R, Gu G D, Koshizuka N, Kendziora C, Jian Sha and Hinks D G 2001 *Phys. Rev. Lett.* **87** 177007
[38] Kaminski A, Randeria M, Campuzano J C, Norman M R, Fretwell H, Mesot J, Sato T, Takahashi T and Kadowaki K 2001 *Phys. Rev. Lett.* **86** 1070
[39] Zasadzinski J F, Ozyuzer L, Miyakawa N, Gray K E, Hinks D G and Kendziora C 2001 *Phys. Rev. Lett.* **87** 067005
[40] Zasadzinski J F, Ozyuzer L, Coffey L, Gray K E, Hinks G D and Kendziora C 2006 *Phys. Rev. Lett.* **96** 017004
[41] Stock C, Buyers W J L, Liang R, Peets D, Tun Z, Bonn D, Hardy W N and Birgeneau R J 2004 *Phys. Rev. B* **69** 014502
[42] Kordyuk A A, Borisenko S V, Zabolotnyy V B, Geck J, Knupfer M, Fink J, Buechner B, Lin C T, Keimer B, Berger H, Komiya Seiki and Ando Yoichi 2005 (*Preprint cond-mat*/0510760)
[43] Demler E. and Zhang Z C 1998 *Nature (London)* **396** 733
[44] Scalapino D J 1999 *Science* **284** 1282
[45] Kee H -Y, Kivelson S A and Aeppli G 2002 *Phys. Rev. Lett.* **88** 257002 and refferences therein
[46] Munzar D, Bernhard C and Cardona M 1999 *Physica C* **317-318** 547
[47] Abanov Ar, Chubukov A V, Eschrig M, Norman M R and Schmalian J 2002 *Phys. Rev. Lett.* **89** 177002
[48] Hwang J, Yang J, Timusk T, Sharapov S G, Carbotte J P, Bonn D A, Liang Ruixing and Hardy W N 2006 *Phys. Rev. B* **73** 014508
[49] Ma Y C and Wang N L 2006 *Phys. Rev. B* **73** 144503
[50] Shibauchi T, Krusin-Elbaum L, Li M, Maley M P and Kes P H 2001 *Phys. Rev. Lett.* **86** 5763
[51] Ozyuzer L, Zasadzinski J F, Gary K E, Kendziora C and Miyakawa N 2002 *Europhys. Lett.* **58** 589
[52] Yoshida T, Zhou X J, Nakamura M, Kellar S A, Bogdanov P V, Lu E D, Lanzara A, Hussain Z, Ino A, Mizokawa T, Fujimori A, Eisaki H, Kim C, Shen Z -X, Kakeshita T and Uchida S 2001 *Phys. Rev. B* **63** 220501
[53] Takeuchi T, Yokoya T, Shin S, Jinno K, Matsuura M, Kondo T, Ikuta H and Mizutani U 2001 *J of Electron Spec. and relat. phenom.* **114-116** 629
[54] Ino A, Kim C, Nakamura M, Yoshida T, Mizokawa T, Fujimori A, Shen Z -X, Kakeshita T, Eisaki H and Uchida S 2002 *Phys. Rev. B* **65** 094504
[55] Kaminski A, Rosenkranz S, Fretwell H M, Norman M R, Randeria M, Campuzano J C, Park J-M, Li Z Z and Raffy H 2006 *Phys. Rev. B* **73** 174511
[56] Takeuchi T, Kondo T, Kitao T, Kaga H, Yang H, Ding H, Kaminski A and Campuzano J C 2005 *Phys. Rev. Lett.* **95** 227004
[57] Varma C M, Littlewood P B and Schmitt-Rink S 1989 *Phys. Rev. Lett.* **63** 1996
[58] Hayden S M, Aeppli G, Dai P, Mook H A, Perring T G, Cheong S -W, Fisk Z, Doan F and Mason T E 1998 *Physica B* **241-243** 765
[59] Lanzara A, Bogdanov P V, Zhou X J, Kellar S A, Feng D L, Lu E D, Yoshida T, Eisaki H, Fujimori A, Kishio K, Shimoyama J -I, Noda T, Uchida S, Hussain Z and Shen Z -X 2001 *Nature (London)* **412** 510
[60] Hwang J, Yang J, Timusk T and Chou F C 2005 *Phys. Rev. B* **72** 024549
[61] Collins R T, Schlesinger Z, Holtzberg F, Chaudhari P and Feild C 1989 *Phys. Rev. B* **39** 6571
[62] Eisaki H, Kaneko M, Feng D L, Damascelli A, Mang P K, Shen K M, Shen Z -X and Greven M 2004 *Phys. Rev. B* **69** 064512
[63] Orenstein J and Rapkine D H 1988 *Phys. Rev. Lett.* **60** 968
[64] Reedyk M and Timusk T 1992 *Phys. Rev. Lett.* **69** 2705
[65] Hwang J, Sills K and Timusk T 2003 (*Unpublished*)
[66] Homes C C, Reedyk M A, Crandles D A and Timusk T 1993 *Applied Optics* **32** 2976
[67] Presland M R, Tallon J L, Buckley R G, Liu R S and FlowerN E 1991 *Phyica C* **176** 95

[68] Hwang J, Timusk T, Puchkov A V, Wang N L, Gu G D, Homes C C, Tu J J and Eisaki H 2004 *Phys. Rev. B* **69** 094520
[69] Wooten Frederick 1972 *Optical Properties of Solids* (New York: Academic)
[70] Santander-Syro A F, Lobo R P S M, Bontemps N, Konstantinovic Z, Li Z and Raffy H 2002 *Phys. Rev. Lett.* **88** 097005
[71] Kuzmenko A B 2005 *Rev. Sci. Instru.* **76** 083108
[72] Terasaki I, Tajima S, Eisaki H, Takagi H, Uchinokura K and Uchida S 1990 *Phys. Rev. B* **41** 865
[73] Mattis D C and Bardeen J 1958 *Phys. Rev.* **111** 412
[74] Tikham M 1975 *Introduction to Superconductivity* (New York: McGraw-Hill)
[75] Leplae L 1983 *Phys. Rev. B* **27** 1191
[76] Zimmermann W, Brandt E H, Bauer M, Seider E and Genzel E 1991 *Physica C* **183** 99
[77] Anderson P W 1997 *Phys. Rev. B* **55** 11785
[78] van der Marel D, Molegraaf H J A, Zaanen J, Nussinov Z, Carbone F, Damascelli A, Eisaki H, Greven M, Kes P H and Li M 2004 *Nature (London)* **425** 271
[79] Anderson P W 2005 (*Preprint cond-mat*/0512471)
[80] Takenaka K, Mizuhashi K, Takagi H, and Uchida S 1994 *Phys. Rev B* **50** 6534
[81] Sutherland M L 2004 *Thesis University of Toronto*
[82] Basov D N, Puchkov A V, Hughes R A, Strach T, Preston J, Timusk T, Bonn D A, Liang R and Hardy W N 1994 *Phys. Rev. B* **49** 12165
[83] Ortolani M, Calvani P and Lupi S 2005 *Phys. Rev. Lett.* **94** 067002
[84] Norman M and Pépin C 2003 *Rep. Prog. Phys.* **66** 1547
[85] Homes C C, Dordevic S V, Bonn D A, Liang Ruixing and Hardy W N 2004 *Phys. Rev. B* **69** 024514
[86] Niedermayer Ch, Bernhard C, Binninger U, Glckler H, Tallon J L, Ansaldo E J and Budnick J I 1993 *Phys. Rev. Lett.* **71** 1764
[87] Villard G, Pelloquin D and Maignan A 1998 *Phys. Rev. B* **58** 15231 and references therein
[88] Allen P B 1971 *Phys. Rev. B* **3** 305
[89] Carbotte J P, Schachinger E and Hwang J 2005 *Phys. Rev. B* **71** 054506
[90] Schachinger E, Tu J J and Carbotte J P 2003 *Phys. Rev. B* **67** 214508
[91] Millis A J and Drew H D 2003 *Phys. Rev. B* **67** 214517
[92] Sharapov S G and Carbotte J P 2005 *Phys. Rev. B* **72** 134506
[93] Shulga S V, Dolgov O V and Maksimov E G 1991 *Physica C* **178** 266
[94] Hwang J, Timusk T and Carbotte J P 2006 (*Preprint*)
[95] Marsiglio F, Startseva T and Carbotte J P 1998 *Phys. Lett. A* **245** 172
[96] Abanov A, Chubukov A V and Schmalian J 2001 *Phys. Rev. B* **63** 180510(R)
[97] Dordevic S V, Homes C C, Tu J J, Valla T, Strongin M, Johnson P D, Gu G D and Basov D N 2005 *Phys. Rev. B* **71** 104529
[98] Padilla W J, Lee Y S, Dumm M, Blumberg G, Ono S, Segawa K, Komiya S and Ando Y 2005 *Phys. Rev. B* **72** 060511
[99] Uemura Y J, Le L P, Luke G M, Sternlieb B J, Wu W D, Brewer J H, Riseman T M, Seaman C L, Maple M B, Ishikawa M, Hinks D G, Jorgensen J D, Saito G and Yamochi H 1991 *Phys. Rev. Lett.* **66** 2665
[100] Basov D N, Woods S I, Katz A S, Singley E J, Dynes R C, Xu M, Hinks D G, Homes C C and Strongin M 1999 *Science* **283** 49
[101] Boris A V, Kovaleva N N, Dolgov O V, Holden T, Lin C T, Keimer B and Bernhard C 2004 *Science* **304** 708
[102] Kuzmenko A B, Molegraaf H J A, Carbone F and van der Marel D 2005 *Phys. Rev. B* **72** 144503
[103] Santander-Syro A F, Lobo R P S M, Bontemps N, Lopera W, Girat D, Konstantinovic Z, Li Z Z and Raffy H 2004 *Phys. Rev. B* **70** 134504